

Article

Analysis and Optimization of Three-Resonator Wireless Power Transfer System for Predetermined-Goals Wireless Power Transmission

Jin Zhang ¹ and Chonghu Cheng ^{2,*}

¹ College of Electronic Science and Engineering, Nanjing University of Posts and Telecommunications, Nanjing 210003, China; zhangjin0655@163.com

² College of Communications and Information Engineering, Nanjing University of Posts and Telecommunications, Nanjing 210003, China

* Correspondence: chengch@njupt.edu.cn; Tel.: +86-25-8349-2430

Academic Editor: Chang Wu Yu

Received: 26 January 2016; Accepted: 25 March 2016; Published: 7 April 2016

Abstract: Three-resonator wireless power transfer (WPT) systems have been proposed to improve the power transfer efficiency (PTE) and power delivered to the load (PDL) in recent years. However, analysis formulas of a three-resonator WPT system are complicated, and the parameters for clarifying the transfer characteristics of this system are difficult to extract. In this paper, concise formulas for analyzing PTE and PDL of the three-resonator system are derived by introducing three factors. Diagram discriminance based on the derived formulas is proposed to obtain the frequency splitting criterions of PTE and PDL in this system. Further, at the transfer distances, where the PTE and PDL are low at original frequency due to frequency splitting phenomenon, the two predetermined-goals of maximizing PTE and PDL are achieved by optimizing coupling strength between the three resonators. The third predetermined-goal of obtaining a constant amount of PDL transfer at maximum PTE is also implemented based on basic algorithms in numerical software. Finally, Simulation and measurement results verify the correctness of analyzing the transfer characteristics of three-resonator WPT system using the presented concise formulas and discriminance. Moreover, effectiveness of realizing the three predetermined-goals via the proposed optimization method is confirmed with experiments.

Keywords: wireless power transfer (WPT); three-resonator system; frequency splitting phenomenon; predetermined-goals

1. Introduction

Several means of wireless power transfer (WPT), including far-field, near-field, capacitive and magnetic coupling, have attracted much attention in recent years [1–6]. In particular, the way of magnetic coupling WPT (MCWPT) has gained rapid development for its high efficiency and strong robustness. To extend the transmission distance of traditional two-resonator MCWPT system further, a method of inserting intermediate resonators (IX) between the transmitter (TX) and the receiver (RX) to form three-resonator system has been proposed recently [7–16]. It has proved in [7] that three-resonator WPT system with IX close to TX or RX can achieve a relatively high power transfer efficiency (PTE) at original resonate frequency compared two-resonator counterpart. Ahn and Hong [8] pointed out that power transmission can be maximized at original resonant frequency via inserting a resonator in traditional two-resonator system. However, the conclusion that power transmission is always maximized at original resonant frequency in a three-resonator system is not entirely accurate, which will be proved in this paper. Although the analysis in [9] has proven the effectiveness of improving energy exchange rate in three-resonator system, the PTE and power delivered to the load (PDL) linking to the energy exchange rate was not quantitatively analyzed. Zhang *et al.* [10] has

indicated that three-resonator WPT system can extend the power transfer distance, compared with traditional two-resonator WPT system. However, the acquisition of the optimal inserting position of IX for maximal PTE lacked theoretical analysis in this reference. Kim *et al.* [11] analyzed the efficiency characteristics of a WPT system with an IX which is coaxially and perpendicularly set to TX (or RX). In [12], due to strong coupling between TX and IX, a small current in TX can be obtained in a three-resonator system, which results in small loss in source resistance and improves PTE in such system. However, all the analyses in [10–12] were limited to original resonant frequency, which cannot reveal the relations between optimal transfer characteristics and system's working frequency. Although resonators with different resonant frequencies have been used in [13] to obtain a constant output current for various load resistor, further works which provide in-depth understanding of power transfer characteristics and guidelines for obtaining predetermined-goals WPT are needed in three-resonator system.

In order to maximize the PTE, optimizing the geometries of coils of TX and RX has been proposed [17–19]. However, the optimized coils with the proper size, turns and conductor width for the maximizing PTE in these references were only effective for a certain transfer distance. A constant amount of PDL need to be transferred at maximum PTE for practical application in a WPT system [20–22]. However, on-chip frequency-tracking oscillation class-D PA in [20] and additional compensation capacitors in [21] have increased the cost and volume of WPT system.

In this work, a detailed analysis of power transfer characteristics of three-resonator WPT *versus* working frequency and the mutual inductances between the three resonators is presented using circuit theory. Furthermore, a design method by adjusting rotation angles of TX and RX, corresponding to optimizing coupling strength between IX and TX (or RX), is used to achieve three predetermined-goals of maximizing PTE transfer, maximizing PDL transfer and a constant PDL transfer at maximum PTE at original frequency. Optimizing coupling coefficients between the resonators instead of optimizing coils' structure and of using additional compensation circuit to implement frequency tracking method can reduce the system cost and complexity to realize the three goals. The outline of this paper is as follows. Section 2 derives analytic formulas of the PTE and PDL for three-resonator system and analyzes the characteristics of PTE and PDL of a case based on practical resonators using diagram discriminance. Section 3 presents the optimization schemes for the three goals. Experimental verification of the analysis results and the effectiveness of proposed optimizing method are given in Section 4. Finally, Section 5 briefly summarizes the contributions of this work.

2. System Analysis

Figure 1a shows the simplified circuit of a magnetic coupling three-resonator WPT system. To concisely derive the analytical expressions of this WPT system, three parameters are introduced: inductance scaling factor, α_{21} and α_{31} ($\alpha_{21} > 0$ and $\alpha_{31} > 0$), expressing as $\alpha_{21}^2 = L_2/L_1$ and $\alpha_{31}^2 = L_3/L_1$; resistance scaling factor, β_{21} and β_{31} ($\beta_{21} > 0$ and $\beta_{31} > 0$), expressing as $\beta_{21}^2 = R_2/R'_S$ and $\beta_{31}^2 = R'_L/R'_S$, where $R'_L = R_3 + R_L$ and $R'_S = R_1 + R_S$; generalized mistuning factor $\omega_v = Q_{S0}(\omega/\omega_0 - \omega_0/\omega)$, where $Q_{S0} = \omega_0 L_1/R'_S$ is loaded quality factor of lossy TX at the resonant frequency ω_0 . The currents I_{TX} , I_{IX} and I_{RX} in TX, IX and RX can be solved by KVL via the following matrix equation:

$$\begin{bmatrix} 1 + j\omega_v & j\alpha_{21}k_{TI}Q_S & j\alpha_{31}k_{TR}Q_S \\ j\alpha_{21}k_{TI}Q_S & \beta_{21}^2 + j\alpha_{21}^2\omega_v & j\alpha_{21}\alpha_{31}k_{IR}Q_S \\ j\alpha_{31}k_{TR}Q_S & j\alpha_{21}\alpha_{31}k_{IR}Q_S & \beta_{31}^2 + j\alpha_{31}^2\omega_v \end{bmatrix} \begin{bmatrix} I_{TX} \\ I_{IX} \\ I_{RX} \end{bmatrix} = \begin{bmatrix} V_S/R'_S \\ 0 \\ 0 \end{bmatrix} \quad (1)$$

where $Q_S = \omega L_1/R'_S$ is the loaded quality factor of lossy TX at working frequency ω , and V_S is root mean square (RMS) amplitude of the sinusoidal voltage source. Since the cross coupling between TX

and RX are usually negligible under the conditions of $k_{TR} \ll k_{TI}$ and $k_{TR} \ll k_{IR}$, the currents I_{TX} , I_{IX} and I_{RX} are calculated from Equation (1) as follows:

$$I_{TX} = \frac{V_S A_2}{R'_S [A_1 - (1 + j\omega_v) A_2]} \tag{2a}$$

$$I_{IX} = \frac{V_S A_1 / (\alpha_{21} k_{TI} Q_S)}{-jR'_S [A_1 - (1 + j\omega_v) A_2]} \tag{2b}$$

$$I_{RX} = \frac{jV_S \alpha_{21}^2 \alpha_{31} k_{TI} k_{IR} Q_S^2}{-jR'_S [A_1 - (1 + j\omega_v) A_2]} \tag{2c}$$

where:

$$A_1 = \alpha_{21}^2 k_{TI}^2 Q_S^2 (\beta_{31}^2 + j\alpha_{31}^2 \omega_v)$$

$$A_2 = \alpha_{21}^2 \alpha_{31}^2 (\omega_v^2 - k_{IR}^2 Q_S^2) - j\omega_v (\alpha_{21}^2 \beta_{31}^2 + \alpha_{31}^2 \beta_{21}^2) - \beta_{21}^2 \beta_{31}^2$$

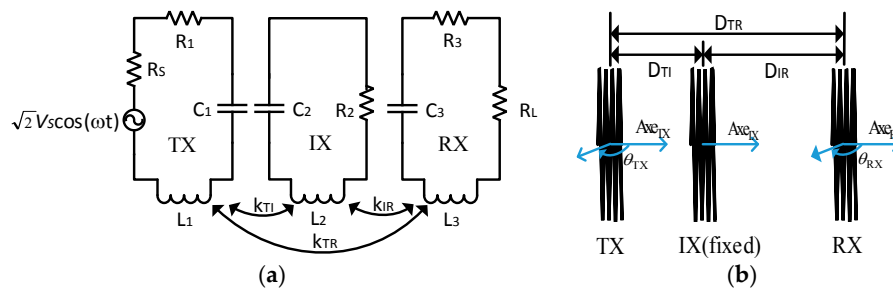


Figure 1. Three-resonator wireless power transfer (WPT) system: (a) Equivalent circuit; and (b) Schematic diagram.

2.1. Transfer Characteristics of Power Transfer Efficiency

The PTE as a function of k_{TI} , k_{IR} and ω is defined as the ratio between the PDL and the total power supplied from the sources:

$$PTE = \frac{R_L |I_{RX}|^2}{R'_S |I_{TX}|^2 + R_2 |I_{IX}|^2 + R'_L |I_{RX}|^2} = \frac{k_{TI}^2 k_{IR}^2 Q_S^4 \beta_L^2 / \alpha_{31}^2}{(\omega_v^2)^2 + b_e \omega_v^2 + c_e} = \frac{k_{TI}^2 k_{IR}^2 \beta_L^2 / \alpha_{31}^2}{F(\omega, k_{TI}, k_{IR})} \tag{3}$$

where:

$$b_e = \beta_{21}^4 / \alpha_{21}^4 + \beta_{31}^4 / \alpha_{31}^4 + k_{TI}^2 Q_S^2 \beta_{21}^2 / \alpha_{21}^2 - 2k_{IR}^2 Q_S^2$$

$$c_e = [\beta_{21}^2 \beta_{31}^2 / (\alpha_{21}^2 \alpha_{31}^2) + k_{IR}^2 Q_S^2]^2 + [\beta_{21}^2 \beta_{31}^2 / (\alpha_{21}^2 \alpha_{31}^2) + k_{IR}^2 Q_S^2] k_{TI}^2 Q_S^2 \beta_{31}^2 / \alpha_{31}^2$$

and load resistance scaling factor β_L ($\beta_L > 0$), $\beta'_L = R_L / R'_S$. In the expression of $F(\omega, k_{TI}, k_{IR}) = [(\omega_v^2)^2 + b_e \omega_v^2 + c_e] / Q_S^4$, ω_v^2 and Q_S are both functions of frequency ω . Obviously, to obtain analytical expression of extremal frequencies for the local extrema of $F(\omega, k_{TI}, k_{IR})$ (or PTE) is difficult. However, if the $F(\omega, k_{TI}, k_{IR})$ value calculated with a constant Q_{SC0} approaches that with the variable Q_S , the extremal frequencies expression can be expressed in terms of Q_{SC0} . Using the resonator with parameters of $R_1 = 5.1 \Omega$, $L_1 = 133 \mu\text{H}$ and resonant frequency $f_0 = 1.96 \text{ MHz}$ as TX, IX and RX, Figure 2a shows the Q_S versus normalized frequency ω / ω_0 . It varies from 144.5 to 176.6 with ω / ω_0 varying from 0.9 to 1.1, and $Q_{S0} = 161$ ($C_{o=0}$) at $\omega = \omega_0$. For comparing, $Q_{S+} = 190$ and $Q_{S-} = 140$ are introduced to calculate $F(\omega, k_{TI}, k_{IR})$. Figure 2b shows function $F(\omega, k_{TI}, k_{IR})$ versus normalized frequency with variable Q_S and the three constant Q_{S0} ($C_{o=0}$, + and -) values at $k_{TI} = 0.0053$, $k_{IR} = 0.0666$, $\alpha_{21}^2 = 1$, $\alpha_{31}^2 = 1$, $\beta_{21}^2 = 0.5$ and $\beta_{31}^2 = 5$. For each quality factor, two local minimums of $F(\omega,$

k_{TL}, k_{IR}), corresponding to local maximums of PTE, occur at both high and low frequency ranges. The locally minimal $F(\omega, k_{TL}, k_{IR})$ values for each case are symbolized as $F_{H-Q_S} (F_{L-Q_S}), F_{H-Q_{S0}} (F_{L-Q_{S0}}), F_{H-Q_{S+}} (F_{L-Q_{S+}})$ and $F_{H-Q_{S-}} (F_{L-Q_{S-}})$ at high (low) frequency range, respectively. The normalized frequencies of the local minimums of $F(\omega, k_{TL}, k_{IR})$ for Q_S, Q_{S0}, Q_{S+} and Q_{S-} are $NF_{H-Q_S} (NF_{L-Q_S}), NF_{H-Q_{S0}} (NF_{L-Q_{S0}}), NF_{H-Q_{S+}} (NF_{L-Q_{S+}})$ and $NF_{H-Q_{S-}} (NF_{L-Q_{S-}})$, respectively. It can be seen that $F_{H-Q_{S0}} (F_{L-Q_{S0}})$ and $NF_{H-Q_{S0}} (NF_{L-Q_{S0}})$ are close to $F_{H-Q_S} (F_{L-Q_S})$ and $NF_{H-Q_S} (NF_{L-Q_S})$ at high (low) frequency range respectively, therefore, we substitute Q_{S0} for Q_S in Equation (3) to study the PTE characteristics. Frequency characteristics of PTE can be analyzed via ω_v only. b_e and c_e are rewritten as b_{e0} and c_{e0} when Q_S is substituted by Q_{S0} . The denominator in Equation (3) is extracted to form a function $f(\omega_v^2)$ in terms of $\omega_v^2, f(\omega_v^2) = (\omega_v^2)^2 + b_{e0}\omega_v^2 + c_{e0}$, obviously $\omega_v^2 \geq 0$. Substituting variable x for ω_v^2 in $f(\omega_v^2)$, the expression is rearranged as a quadratic function of $x, f(x) = x^2 + b_{e0}x + c_{e0}$, where $x \in (-\infty, \infty)$, which is used to investigate the local extrema of quadratic function with one variable in mathematics. $f'(x)$ is the derivative of $f(x)$ with respect to $x: f'(x) = 2x + b_{e0}$. $x_0 = -b_{e0}/2$ obtained by solving $f'(x) = 0$ is the point for minimum $f(x)$. From Equation (3), it can be seen that PTE maximizes when $f(\omega_v^2)$ minimizes. Properties of $f(x)$ and frequency splitting situations of PTE are analyzed using diagram discriminance in Table 1.

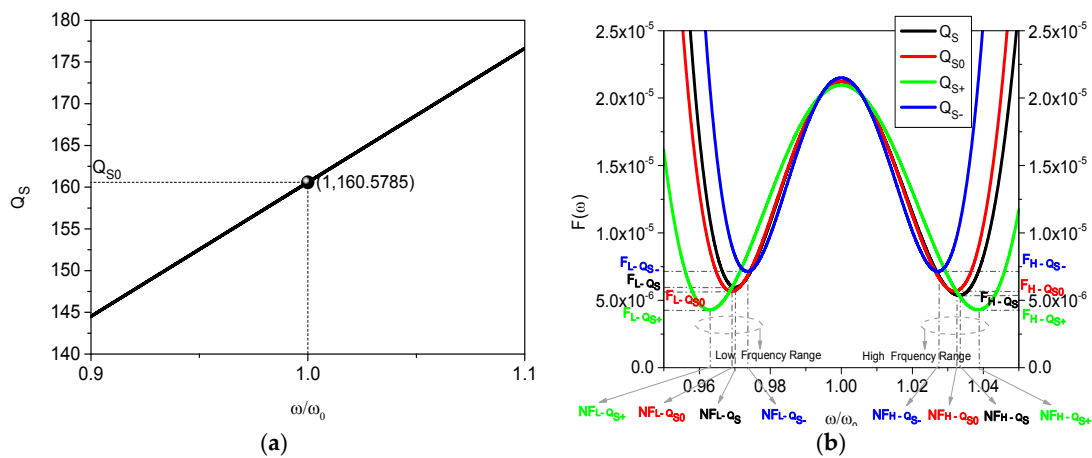
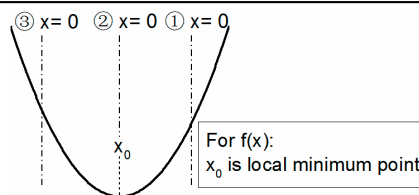


Figure 2. (a) Loaded Q -factor of lossy TX vs. ω/ω_0 ; and (b) $F(\omega, k_{TL}, k_{IR})$ for investigating PTE vs. ω/ω_0 with various loaded Q -factor under $k_{TL} = 0.0053, k_{IR} = 0.0666, \alpha_{21}^2 = \alpha_{31}^2 = 1, \beta_{21}^2 = 0.5$ and $\beta_{31}^2 = 5$.

Table 1. Properties and graph of $f(x) = x^2 + b_{e0}x + c_{e0}$ for analyzing power transfer efficiency (PTE).

Locations of x_0	① $x_0 < 0$	② $x_0 = 0$	③ $x_0 > 0$
Local minimum of $f(\omega_v^2), \omega_v^2 \geq 0$ in this paper	$f(\omega_v^2 = 0)$	-	$f(\omega_v^2 = x_0)$
Coupling region for PTE	Non-frequency splitting region	Critical frequency splitting	Frequency splitting region
Number of local maximum for PTE	1	-	2

Graph and extrema for $f(x)$, where $x \in (-\infty, \infty)$



From Table 1, PTE maximizes at $\omega_v^2 = 0$, namely $\omega = \omega_0$, when $x_0 < 0$, the corresponding coupling region of PTE is named non-frequency splitting region. Using $\omega_v^2 = x_0$, the two splitting frequencies, $\omega_{e-H/L}$, for maximum PTE can be derived in frequency splitting region, where $x_0 > 0$.

$$\omega_{e-H/L} = \omega_0 \sqrt{1 + \frac{x_0}{2Q_{S0}^2} \pm \frac{\sqrt{x_0(x_0 + 4Q_{S0}^2)}}{2Q_{S0}^2}} \tag{4}$$

By substituting $\omega_v^2 = 0$ into Equation (3), The PTE at original frequency, PTE_0 , can be presented as:

$$PTE_0 = \frac{k_{TI}^2 k_{IR}^2 Q_{S0}^4 \beta_L^2 / \alpha_{31}^2}{\left[\beta_{21}^2 \beta_{31}^2 / (\alpha_{21}^2 \alpha_{31}^2) + k_{IR}^2 Q_{S0}^2 \right]^2 + \left[\beta_{21}^2 \beta_{31}^2 / (\alpha_{21}^2 \alpha_{31}^2) + k_{IR}^2 Q_{S0}^2 \right] k_{TI}^2 Q_{S0}^2 \beta_{31}^2 / \alpha_{31}^2} \tag{5}$$

2.2. Transfer Characteristics of Power Delivered to the Load

Magnitude of induced current in RX, $|I_{RX}|$, can present the characteristics of PDL because of $PDL = R_L |I_{RX}|^2$. $|I_{RX}|$ is compiled according to Equation (2c) as follow:

$$|I_{RX}| = \frac{V_S k_{TI} k_{IR} Q_S^2}{R'_S \alpha_{31} \sqrt{(\omega_v^2)^3 + b_p (\omega_v^2)^2 + c_p \omega_v^2 + d_p}} \tag{6}$$

where:

$$b_p = \beta_{21}^4 / \alpha_{21}^4 + \beta_{31}^4 / \alpha_{31}^4 + 1 - 2Q_S^2 (k_{TI}^2 + k_{IR}^2)$$

$$c_p = (k_{TI}^2 + k_{IR}^2)^2 Q_S^4 / (\alpha_{21}^2 \alpha_{31}^2) + 2Q_S^2 \left\{ (\beta_{21}^2 / \alpha_{21}^2 - \beta_{31}^2 / \alpha_{31}^2) k_{TI}^2 + [\beta_{21}^2 \beta_{31}^2 / (\alpha_{21}^2 \alpha_{31}^2) - 1] k_{IR}^2 \right\} + \beta_{21}^4 / \alpha_{21}^4 + \beta_{31}^4 / \alpha_{31}^4 + \beta_{21}^4 \beta_{31}^4 / (\alpha_{21}^4 \alpha_{31}^4)$$

$$d_p = \left[\left(k_{TI}^2 \beta_{31}^2 / \alpha_{31}^2 + k_{IR}^2 \right) Q_S^2 + \beta_{21}^2 \beta_{31}^2 / (\alpha_{21}^2 \alpha_{31}^2) \right]^2$$

For the same reason as PTE in Equation (3), all Q_S in Equation (6) can be substituted by Q_{S0} . b_p and c_p are rewritten as b_{p0} and c_{p0} when Q_S is substituted by Q_{S0} . The expression under the square root sign is extracted to form a function $g(\omega_v^2)$ in term of ω_v^2 , $g(\omega_v^2) = (\omega_v^2)^3 + b_{p0} (\omega_v^2)^2 + c_{p0} \omega_v^2 + d_{p0}$, obviously $\omega_v^2 \geq 0$. Substituting variable x for ω_v^2 in $g(\omega_v^2)$, the expression is rearranged as a cubic function of x , $g(x) = x^3 + b_{p0} x^2 + c_{p0} x + d_{p0}$, where $x \in (-\infty, \infty)$, which is used to investigate the local extrema of cubic function with one variable in mathematics. $g'(x)$ is the derivative of $g(x)$ with respect to x : $g'(x) = 3x^2 + 2b_{p0} x + c_{p0}$ and $\Delta = (2b_{p0})^2 - 4(3c_{p0})$, where factor Δ is used to judge whether there are local extrema or not for $g(x)$.

Two cases of $\Delta > 0$ and $\Delta = 0$ are listed in Table 2 for illuminating the characteristics of $g(x)$ and frequency splitting situations of $|I_{RX}|$ (or PDL). x_1 and x_2 obtained by solving $g'(x) = 0$ are the stationary points for $g(x)$ when $\Delta \geq 0$:

$$x_1 = \left(-b_{p0} - \sqrt{b_{p0}^2 - 3c_{p0}} \right) / 3 \tag{7a}$$

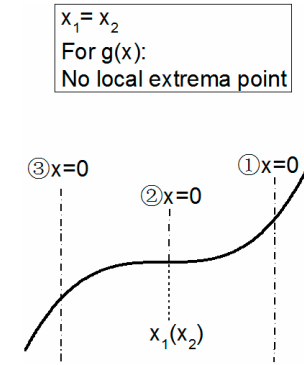
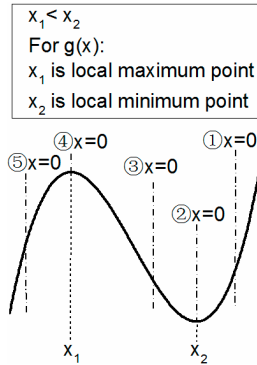
$$x_2 = \left(-b_{p0} + \sqrt{b_{p0}^2 - 3c_{p0}} \right) / 3 \tag{7b}$$

Table 2. Properties and graphs of $g(x) = x^3 + b_{p0}x^2 + c_{p0}x + d_{p0}$ for analyzing $|I_{RX}|$ (or power delivered to the load (PDL)).

Scope of Δ	$\Delta > 0$					$\Delta = 0$	
	① $x_1 < x_2 < 0$	② $x_1 < x_2 = 0$	③ $x_1 < 0 < x_2$	④ $0 = x_1 < x_2$	⑤ $0 < x_1 < x_2$	① ② $0 \geq x_1 = x_2$	③ $0 < x_1 = x_2$
Locations of x_1 and x_2	① $x_1 < x_2 < 0$	② $x_1 < x_2 = 0$	③ $x_1 < 0 < x_2$	④ $0 = x_1 < x_2$	⑤ $0 < x_1 < x_2$	① ② $0 \geq x_1 = x_2$	③ $0 < x_1 = x_2$
Local minimum of $g(\omega_v^2)$, $\omega_v^2 \geq 0$ in this paper	$g(\omega_v^2 = 0)$	-	$g(\omega_v^2 = x_2)$	-	$g(\omega_v^2 = 0)$ and $g(\omega_v^2 = x_2)$	$g(\omega_v^2 = 0)$	-
Coupling regions for I_{RX}	Non-frequency splitting region	Critical condition 1 ¹	Frequency splitting region	Critical condition 2 ²	Frequency splitting region	Non-frequency splitting region	Critical condition 3 ³
Frequency number of local maximum for I_{RX}	1	-	2	-	3	1	-

¹ Critical coupling condition for judging the border between non-frequency splitting region and frequency splitting region with two splitting frequencies. ² Critical coupling condition for judging the border between frequency splitting region with two splitting frequencies and with three splitting frequencies. ³ Critical coupling condition for judging the border between non-frequency splitting region and frequency splitting region with three splitting frequencies.

Graphs and extrema for $g(x)$, where $x \in (-\infty, \infty)$



From Equation (6), it can be seen that $|I_{RX}|$ maximizes when $g(\omega_v^2)$ minimizes. If $\Delta > 0$ and $x_1 < x_2 < 0$, $|I_{RX}|$ maximizes only at $\omega_v^2 = 0$, the frequency number of local maximums of $|I_{RX}|$ is one and its coupling region names non-frequency splitting region; if $\Delta > 0$ and $x_1 < 0 < x_2$, $|I_{RX}|$ maximizes only at $\omega_v^2 = x_2$, the frequency number of local maximums of $|I_{RX}|$ is two and its coupling region names frequency splitting region; if $\Delta > 0$ and $0 < x_1 < x_2$, $|I_{RX}|$ maximizes at $\omega_v^2 = x_2$ and $\omega_v^2 = 0$, the frequency number of local maximums of $|I_{RX}|$ is three and its coupling region names frequency splitting region; if $\Delta = 0$ and $0 \geq x_1 = x_2$, $|I_{RX}|$ maximizes only at $\omega_v^2 = 0$, the frequency number of local maximums of $|I_{RX}|$ is one and its coupling region names non-frequency splitting region; if $\Delta < 0$, $g'(x) = 0$ has no solution and $|I_{RX}|$ always maximizes at $\omega_v^2 = 0$, the frequency number of local maximums of $|I_{RX}|$ is one and its coupling region names non-frequency splitting region. There are three kinds of critical point to define the frequency splitting regions of $|I_{RX}|$: one occurs when $\Delta > 0$ and $x_1 < x_2 = 0$, it is the critical point for differentiating between non-frequency splitting region and frequency splitting region with two splitting frequencies; one occurs when $\Delta > 0$ and $0 = x_1 < x_2$, it is the critical point for differentiating between frequency splitting region with two splitting frequencies and frequency splitting region with three splitting frequencies; one occurs when $\Delta = 0$ and $0 < x_1 = x_2$, it is the critical point for differentiating between non-frequency splitting region and frequency splitting region with three splitting frequencies. The two splitting frequencies, $\omega_{p-H/L}$, in frequency splitting region deviating from ω_0 , can be obtained by solving $\omega_v^2 = x_2$.

$$\omega_{p-H/L} = \omega_0 \sqrt{1 + \frac{x_2}{2Q_0^2} \pm \frac{\sqrt{x_2(x_2 + 4Q_0^2)}}{2Q_0^2}} \tag{8}$$

By substituting $\omega_v^2 = 0$ into Equation (6), The $|I_{RX}|$ at original frequency, $|I_{RX}|_0$, can be presented as:

$$|I_{RX}|_0 = \frac{V_S k_{TI} k_{IR} Q_{S0}^2}{R'_S \alpha_{31} \left[(k_{TI}^2 \beta_{31}^2 / \alpha_{31}^2 + k_{IR}^2) Q_{S0}^2 + \beta_{21}^2 \beta_{31}^2 / (\alpha_{21}^2 \alpha_{31}^2) \right]} \tag{9}$$

As for multi-resonator system, the expressions of PTE and PDL can be derived by reflected impedance method [14–16]. Compared with these references, the characteristics of PTE and PDL with respect to non-original frequency, related to ω_v , are considered in our study. Based on reflected impedance method, the expressions of PTE and PDL for n -resonator system are $n - 1$ and n order function of ω_v^2 , respectively.

2.3. Theoretical Illumination with a Case Based on Practical Resonators

In this section, a case is presented to clarify the analysis in Sections 2.1 and 2.2. To reveal the transfer characteristics in terms of the transmission distance, the coupling coefficients calculated in the aforementioned procedure need to be transformed into transmission distance first. The mutual inductance equation proposed in [23] is revamped in this paper for two single layer coils with inclined axes (Figure 3) as follow:

$$M = \frac{N_1 N_2 \sum_{g=-m_1}^{g=m_1} \sum_{p=-m_2}^{p=m_2} M(g, p)}{(2m_1 + 1)(2m_2 + 1)} \tag{10}$$

where:

$$M(g, p) = \frac{\mu_0 \sqrt{r_1 r_2}}{\pi} \int_0^\pi \left[\frac{\cos\theta - \frac{y(p)}{r_2} \cos\phi}{\sqrt{V^3}} \right] \Psi(k) d\phi$$

$$V = \sqrt{1 - \cos^2\phi \sin^2\theta - \frac{2y(p)}{r_2} \cos\phi \cos\theta + \frac{y^2(p)}{r_2^2}}$$

$$\Psi(k) = \left(\frac{2}{k} - k\right) \mathbf{K}(k) - \frac{2}{k} \mathbf{E}(k)$$

$$y(p) = S + \frac{H_2 \sin \theta}{(2m_2 + 1)} p; \quad p = -m_2, \dots, 0, \dots, m_2 \quad (11)$$

$$k^2 = \frac{4r_2 V}{r_1 \left[\left(1 + \frac{r_2 V}{r_1}\right)^2 + \left(\frac{z(g, p)}{r_1} - \frac{r_2 \cos \phi \sin \theta}{r_1}\right)^2 \right]}$$

$$z(g, p) = D + \frac{H_1}{2m_1 + 1} g - \frac{H_2 \cos \theta}{2m_2 + 1} p;$$

$$g = -m_1, \dots, 0, \dots, m_1; \quad p = -m_2, \dots, 0, \dots, m_2$$

H_i , r_i and N_i are the height, radius and turn number of coil i ($i = 1, 2$). D and S are the longitudinal and transverse distances between coils' centers, respectively. θ is the angle between coil planes. m_1 and m_2 are the subdivision number for the height of Coils 1 and 2. $\mathbf{K}(k)$ and $\mathbf{E}(k)$ are complete elliptic integrals of the first and second kind, respectively.

$$\mathbf{K}(k) = \int_0^{\pi/2} \frac{1}{\sqrt{1 - k^2 \sin^2 \xi}} d\xi; \quad \mathbf{E}(k) = \int_0^{\pi/2} \sqrt{1 - k^2 \sin^2 \xi} d\xi \quad (12)$$

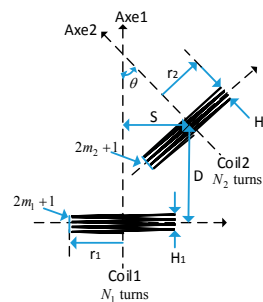


Figure 3. Schematic of two coils for mutual inductance calculation.

Large values of m_1 and m_2 increase the calculation accuracy of mutual inductance. In this study, we calculate with $m_1 = m_2 = 5$ and $S = 0$ m.

We use three identical resonators, which consist of identical coils and series lumped capacitors, to serve as the TX, IX and RX respectively. The parameters of the real resonator are as follows: the multi-strand Litz wire is used to construct the coils, its structures is $\varnothing 0.1$ mm \times 80 strands and overall outer diameter is $\varnothing 1.18$ mm; the radius, height and turn number of the coil are 15.75 cm, 1.5 cm and 11, respectively. The measured value of self-inductance is 133 μ H, total parasitic resistance is 5.1 Ω , and original resonant frequency of the resonator is 1.96 MHz. The parameters for the sample case are: $R'_S = 10.2$ Ω , $\alpha_{21}^2 = \alpha_{31}^2 = 1$, $\beta_{21}^2 = 0.5$, $\beta_{31}^2 = 5$, $\beta_L^2 = 4.5$ ($R_S = 5.1$ Ω , $R_L = 45.9$ Ω) and $V_S = 10$ V, the distance between TX and RX, D_{TR} , is fixed at 70 cm, and the distance between IX and TX, D_{TI} , changes from 10 cm to 60 cm.

Figure 4a shows the judgment conditions of x_j ($j = 0, 1$ and 2) and Δ for frequency splitting for PTE and $|I_{RX}|$ of the sample case. Combining x_0 in this figure with frequency splitting discriminance in Table 1, it can be found that PTE is in the non-frequency splitting region, critical frequency splitting position and frequency splitting region when $D_{TI} <, =$ and > 0.408 m, respectively. Ignoring the cross coupling between TX and RX, the values of PTE versus distance and frequency are shown in Figure 5a. The frequencies for local maximum (FLM) of PTE under different D_{TI} , shown as black lines, are achieved by Equation (4). The frequencies for maximum (FM) of PTE are obtained by searching the

maximum in global frequency domain at each D_{TI} , shown as white dotted lines. It can be seen that the critical frequency splitting distance is at 0.408 m, which validates the analysis result of judging the position for frequency splitting. The FM matches well with the FLM in non-frequency splitting region where $D_{TI} < 0.408$ m, and is very close to the FLM at high splitting frequency in frequency splitting region where $D_{TI} > 0.408$ m. In the greater degree of frequency splitting region, *i.e.*, the region of splitting frequencies keeping farther away from each other, the FM slightly deviates from FLM, seeing the distribution of white dotted line and black line at larger D_{TI} in Figure 5a. The reason is that the splitting frequencies are calculated under the constant Q_{S0} . The values of PTE *versus* distance and frequency with considering cross coupling are shown in Figure 5b. The FM is off FLM slightly to low frequency in non-frequency splitting region because of the effect of cross coupling. In frequency splitting region, the FM is close to the FLM at low splitting frequency under the effect of cross coupling. Comparing Figure 5a,b, the transfer distances for maximal PTE for with and without considering cross coupling are the same. All these show that the analytical solutions obtained by simplified model, namely model ignoring cross coupling, can well show the transfer characteristics of practical complete model, namely model considering cross coupling.

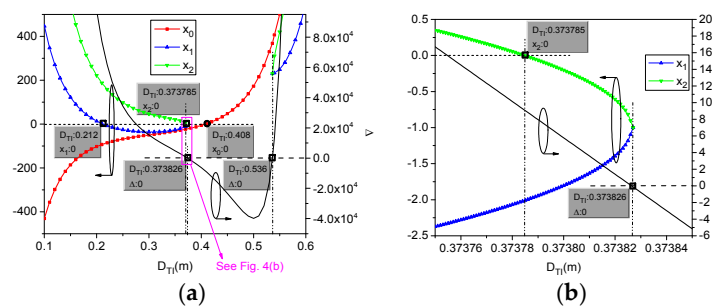


Figure 4. Parameters for judging transfer regions for PTE and PDL ($|I_{RX}|$) when $D_{TR} = 0.7$ m: (a) x_j ($j = 0, 1$ and 2) and Δ vs. D_{TI} from 0.1 m to 0.6 m; and (b) x_j ($j = 1$ and 2) and Δ vs. local D_{TI} .

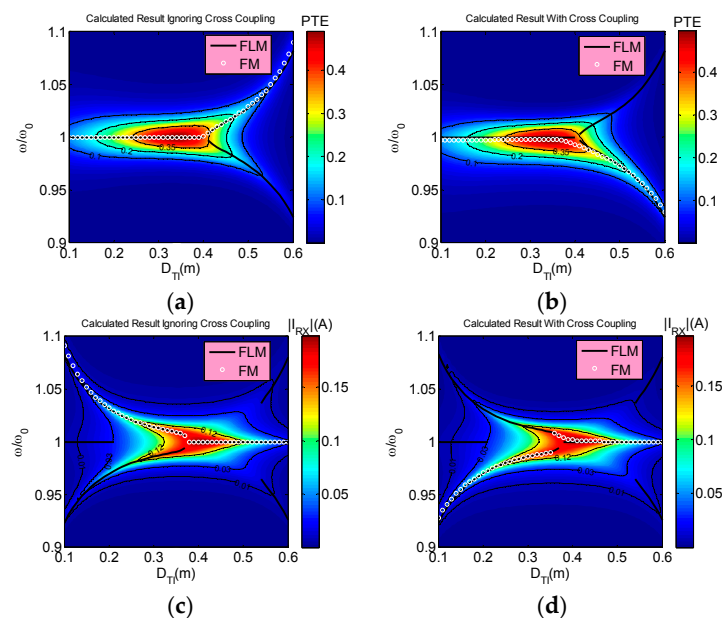


Figure 5. Simulated values of PTE and $|I_{RX}|$ as functions of frequency and transmission distance, D_{TI} , when $D_{TR} = 0.7$ m: (a) PTE vs. ω/ω_0 and D_{TI} under ignoring cross coupling; (b) PTE vs. ω/ω_0 and D_{TI} under considering cross coupling; (c) $|I_{RX}|$ vs. ω/ω_0 and D_{TI} under ignoring cross coupling; and (d) $|I_{RX}|$ vs. ω/ω_0 and D_{TI} under considering cross coupling.

Combining x_1 , x_2 and Δ in Figure 4 and frequency splitting discriminance in Table 2 with the analysis in Section 2.2, we can see: $|I_{RX}|$ is in the non-frequency splitting region when $0.373785 < D_{TI} < 0.373826$ m ($\Delta > 0$, $x_1 < x_2 < 0$), $D_{TI} = 0.373826$ m ($\Delta = 0$, $x_1 = x_2 < 0$) and $0.373826 < D_{TI} < 0.536$ m ($\Delta < 0$); $|I_{RX}|$ is in the frequency splitting region with two splitting frequencies when $0.212 < D_{TI} < 0.373785$ m ($\Delta > 0$, $x_1 < 0 < x_2$); $|I_{RX}|$ is in the frequency splitting region with three splitting frequencies when $D_{TI} < 0.212$ m and $D_{TI} > 0.536$ m ($\Delta > 0$, $0 < x_1 < x_2$). $D_{TI} = 0.373785$ m is the critical coupling distance between non-frequency region and frequency region with two splitting frequencies ($\Delta > 0$, $x_1 < x_2 = 0$); $D_{TI} = 0.212$ m is the critical coupling distance between frequency region with two splitting frequencies and frequency region with three splitting frequencies ($\Delta > 0$, $0 = x_1 < x_2$); $D_{TI} = 0.536$ m is the critical coupling distance between non-frequency region and frequency region with three splitting frequencies ($\Delta = 0$, $0 < x_1 = x_2$). Ignoring the cross coupling between TX and RX, the transfer characteristics of $|I_{RX}|$ versus distance and frequency are shown in Figure 5c. Plotting $|I_{RX}|$ instead of PDL in this figure is that the color gradation of the former is much clearer than the latter in two-dimensional color image. The distributions of $|I_{RX}|$ well verify the analysis of frequency splitting situation. At f_0 , The FM of $|I_{RX}|$ matches well with FLM which is obtained by Equation (8) in non-frequency splitting region ($0.373785 < D_{TI} < 0.536$ m) and frequency splitting region with three splitting frequencies ($D_{TI} > 0.536$ m), and it is very close to the FLM at high splitting frequency in frequency splitting region with two and three splitting frequencies ($0.212 < D_{TI} < 0.373785$ m and $D_{TI} < 0.212$ m). Figure 5d shows the values of $|I_{RX}|$ considering the cross coupling. One major difference from Figure 5c ignoring the cross coupling is that FM in Figure 5d is close to the FLM at low splitting frequency in the two kinds of frequency splitting regions ($0.212 < D_{TI} < 0.373785$ m and $D_{TI} < 0.212$ m). Comparing the simulated values of simplified model in Figure 5c and complete model in Figure 5d, the maximal $|I_{RX}|$ of them and the transfer distance for the maximal $|I_{RX}|$ of them are basically the same.

By this case and the theoretical analysis in this section, we can found that PTE of three-resonator WPT system has at most two splitting frequencies and PDL ($|I_{RX}|$) has at most three splitting frequencies.

3. Optimization for Predetermined-Goals Wireless Power Transmission

Via the analysis in Section 2, we can see that frequency splitting for PTE and PDL takes place when IX gets close to TX or RX, which cause the PTE and PDL decrease at original resonant frequency, f_0 . In this section, we adjust k_{TI} and k_{IR} to obtain three kinds of predetermined-goal WPT at f_0 for different inserted distance, D_{TI} : maximizing PTE transfer; maximizing PDL transfer; obtaining a constant amount of PDL transfer at maximum PTE. MATLAB optimization toolbox is used to determine the k_{TI} and k_{IR} for the three kinds of optimization goals. The frequency tracking method, used in [24,25] to maximize the PTE and PDL, is also presented in this section for comparing.

3.1. Setting the Optimization Goals

As mentioned in Section 2, analytical Equations (3) and (6) of simplified model are competent to reveal the real transfer characteristics of complete model when cross coupling between TX and RX can be ignored ($k_{TR} \ll k_{TI}$ and $k_{TR} \ll k_{IR}$). Equations (5) and (9) as functions of tuning coupling coefficient vector \mathbf{k} , $\mathbf{k} = [k_{TI}, k_{IR}]$, are used to define the optimization functions for the three kinds of predetermined-goal at f_0 . There is a maximum value for \mathbf{k} , i.e., $\mathbf{k}_{\max} = [k_{TI,\max}, k_{IR,\max}]$, for a certain relative positions of TX, IX and RX, when the axes of them are arranged collinearly, namely Axe_{TX} , Axe_{IX} and Axe_{RX} in Figure 1b are collinear, corresponding to $\theta_{TX} = \theta_{RX} = 0^\circ$. By using solver f_{\mincon} in MATLAB, the objective optimization function and constrains of the three predetermined-goals are denoted as following:

Maximizing PTE transfer:

$$\begin{aligned} \min fun_1(\mathbf{k}) &= 1 - PTE_0 \\ \text{s.t. } \mathbf{k} &\leq \mathbf{k}_{\max} \end{aligned} \quad (13)$$

Maximizing PDL transfer:

$$\begin{aligned} \min fun_2(\mathbf{k}) &= -(|I_{RX}|_0)^2 R_L \\ \text{s.t. } \mathbf{k} &\leq \mathbf{k}_{\max} \end{aligned} \quad (14)$$

Obtaining a constant amount of PDL transfer at maximum PTE:

$$\begin{aligned} \min fun_3(\mathbf{k}) &= 1 - PTE_0 \\ \text{s.t. } \begin{cases} \mathbf{k} \leq \mathbf{k}_{\max} \\ |PDL - PDL_C| = 0 \end{cases} \end{aligned} \quad (15)$$

where PDL_C is a constant amount of PDL, according to the requirement of charged devices, for the third optimal goal.

3.2. Numerical Results

The case, analyzed in Section 2.3, is used for the numerical calculation to clarify the feasibility of the optimization method for the first two predetermined-goals. The PTE curves of collinear axes arrangement of the three resonators at f_0 , maximizing PTE using optimizing k at f_0 , and maximizing PTE using frequency tracking method are shown in Figure 6a. The maximal coupling coefficient vector, $\mathbf{k}_{\max} = [k_{TI,\max}, k_{IR,\max}]$, and optimal coupling coefficient vector, $\mathbf{k} = [k_{TI}, k_{IR}]$, for maximizing PTE for each inserting distance, D_{TI} , are plotted in Figure 6b. It can be seen that the values of PTE obtained by optimizing k are equal to those of collinear axes arrangement scenario and frequency tracking method when $D_{TI} < 0.37$ m. This can be explained by the fact that the local maximal PTE only takes place at f_0 when IX gets close to TX (Figure 5a,b). PTE values of frequency tracking method are higher than those of collinear axes arrangement scenario when IX moves over 4.1 m, which is the frequency splitting distance for PTE, actually the accurate splitting distance shown in Figure 4 is 4.08 m. For the inserting distances of IX close to RX, optimizing k for maximal PTE method obtains higher PTE than frequency tracking method and collinear axes arrangement scenario, for instance the former can improve the PTE by up to 10% and 18% comparing with the latter two at $D_{TI} = 0.5$ m, respectively. The PTE values of maximizing PDL via optimizing k , which are always lower than those of maximizing PTE at each D_{TI} , are also compared in Figure 6a. The optimal k_{TI} for maximizing PTE always maintains the maximum value, $k_{TI,\max}$, at whole D_{TI} , while the optimal k_{IR} gradually deviates from $k_{IR,\max}$ to lower value starting at distance $D_{TI} = 0.37$ m. The reason for this optimal k is that the strength of $k_{TI,\max}$ is not enough high to cause frequency splitting when IX moves to TX in collinear axes arrangement scenario while the frequency splitting takes place with increasing $k_{IR,\max}$ when IX moves to RX.

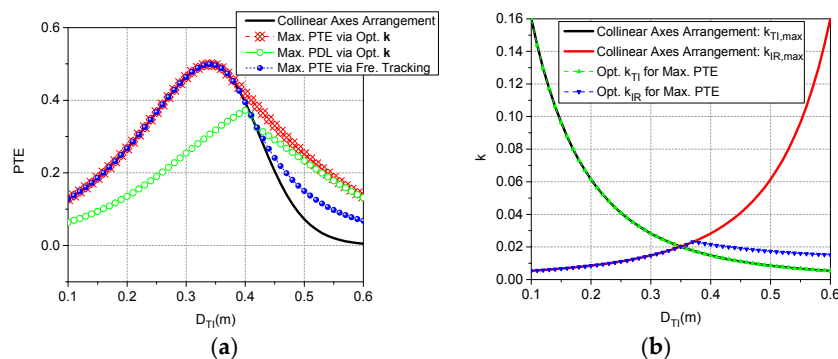


Figure 6. (a) Comparison between maximizing PTE goal by optimizing coupling coefficient vector, \mathbf{k} , and three other power transfer scenarios; (b) Comparison between maximal coupling coefficient vector, $[k_{TI,\max}, k_{IR,\max}]$, of collinear axes arrangement scenario and optimal coupling coefficient vector, $[k_{TI}, k_{IR}]$, for maximizing PTE goal.

In Figure 7a, PDL of maximizing PDL goal by optimizing k at f_0 is compared with PDLs of collinear axes arrangement scenario at f_0 , maximizing PTE goal by optimizing k at f_0 and maximizing PDL goal by frequency tracking method. As in non-frequency splitting region, $0.373785 < D_{TI} < 0.536$ m (Figure 4a,b), and near RX frequency splitting region, $0.536 < D_{TI} < 0.6$ m (Figure 4a), the maximal PDL remains at f_0 (Figure 5c,d), the PDLs obtained via maximizing PDL goal by frequency tracking method are the same with those of collinear axes arrangement scenario when $0.373785 < D_{TI} < 0.6$ m (Figure 7a). While the PDLs of maximizing PDL goal by frequency tracking method are higher than those of collinear axes arrangement scenario in near TX frequency splitting region, $0.1 < D_{TI} < 0.373785$ m (Figure 4a), due to the maximal PDLs occurring at low splitting frequency in this region (Figure 5d). Compared with collinear axes arrangement scenario and maximizing PDL goal by frequency tracking method, the maximizing PDL goal by optimizing k can improve PDLs both below and above the position of $D_{TI} = 0.41$ m. The corresponding tuning k for maximizing PDL goal are compared with the k_{\max} for collinear axes arrangement scenario in Figure 7b. It can be found that decreasing k_{TI} properly under $D_{TI} < 0.41$ m and decreasing k_{IR} properly under $D_{TI} > 0.41$ m can improve the PDL at f_0 . The PDLs of maximizing PTE goal by optimizing k , which are comparatively plotted in Figure 7a, are always lower than those of maximizing PDL goal by optimizing k .

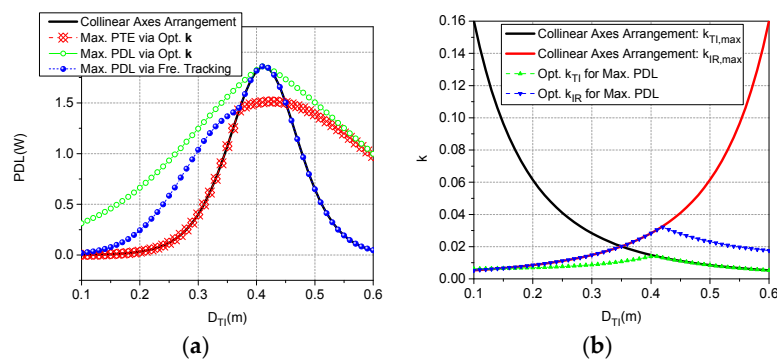


Figure 7. (a) Comparison between maximizing PDL goal by optimizing coupling coefficient vector, k , and three other power transfer scenarios. (b) Comparison between maximal coupling coefficient vector, $[k_{TI,\max}, k_{IR,\max}]$, of collinear axes arrangement scenario and optimal coupling coefficient vector, $[k_{TI}, k_{IR}]$, for maximizing PDL goal.

The third predetermined-goal of obtaining a constant amount of PDL transfer at maximum PTE is instanced under transfer distances $D_{TR} = 0.5, 0.7$ and 0.9 m respectively. The source and load resistance values and resonators used for this optimizing goal are the same with the case for the first two predetermined-goals; the constant PDL_C is set as 0.5 W in this goal. According to the optimization function and constrains in Equation (15), PTEs of this goal by optimizing k are compared with those of maximizing PTE goal by optimizing k and collinear axes arrangement scenario in Figure 8a; and PDLs of this goal by optimizing k are compared with those of maximizing PDL goal by optimizing k and collinear axes arrangement scenario in Figure 8b. It is clear from Figure 8b that the constant $PDL = 0.5$ W can be obtained with $0.1 \text{ m} \leq D_{TI} \leq 0.4 \text{ m}$, $0.16 \text{ m} \leq D_{TI} \leq 0.6 \text{ m}$ and $0.36 \text{ m} \leq D_{TI} \leq 0.72 \text{ m}$ for $D_{TR} = 0.5, 0.7$ and 0.9 m respectively. It is also worth pointing out that no matter how the k is tuned, PDL cannot achieve the power of 0.5 W when $D_{TI} < 0.16$ m for $D_{TR} = 0.7$ m and $D_{TI} < 0.36$ m and $D_{TI} > 0.72$ m for $D_{TR} = 0.9$ m. The lower bound of $D_{TI} = 0.16$ m for 0.5 W in $D_{TR} = 0.7$ m case and lower (upper) bound of $D_{TI} = 0.36$ (0.72) m for 0.5 W in $D_{TR} = 0.9$ m case are determined by the maximizing PDL goal by optimizing k . For $D_{TR} = 0.5, 0.7$ and 0.9 m cases, the PTEs are maximized at $D_{TI} = 0.21, 0.31$ and 0.42 m, respectively, where the corresponding collinear axes arrangement scenarios achieve the PDL values of 0.5 W. For $D_{TR} = 0.5, 0.7$ and 0.9 m cases, the optimal values of k for obtaining a constant PDL transfer at maximum PTE, comparing with those of collinear axes arrangement scenario, are shown in Figure 8c.

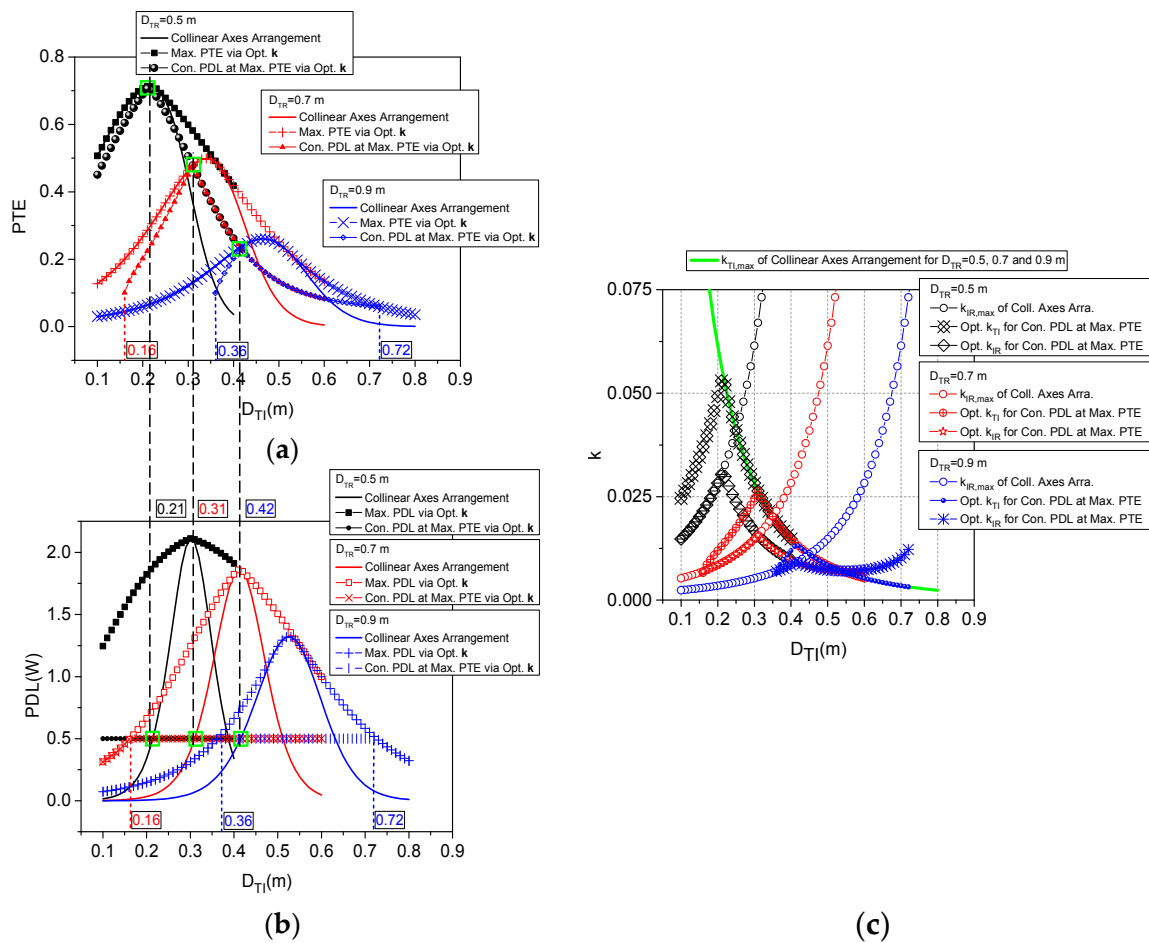


Figure 8. Predetermined-goal of obtaining a constant PDL of 0.5 W at maximum PTE by optimizing coupling coefficient vector, k , in three-resonator WPT: (a) PTEs of collinear axes arrangement scenario, maximizing PTE goal by optimizing k and obtaining a constant PDL at maximum PTE by optimizing k ; (b) PDLs of collinear axes arrangement scenario, maximizing PDL goal by optimizing k and obtaining a constant PDL at maximum PTE by optimizing k ; and (c) values of k for collinear axes arrangement scenario and obtaining a constant PDL at maximum PTE.

4. Experimental Verification

In this section, we discuss the experimental verification of the theoretical analysis and calculation presented in Section 2 and the numerical optimization results of the three predetermined-goals shown in Section 3.2.

4.1. Experimental Setup

The power transfer characteristics of the three-resonator system developed in this work are tested with the aid of the two-port VNA, as shown in Figure 9a. The part number of this VNA is E5071C, Agilent ENA series. The angle vector, $\theta = [\theta_{TX}, \theta_{RX}]$ shown in Figures 1b and 9a, is tuned to achieve the optimal k for the three predetermined-goals WPT. According to the measured S-parameters based on port impedance $z_0 = 50 \Omega$ of the network analyzer, the PDL (or I_{RX}) and PTE of the WPT network with arbitrary R_S and R_L values can be determined by transforming calculation method [22,26], and the block diagram for the procedures is presented in Figure 9b.

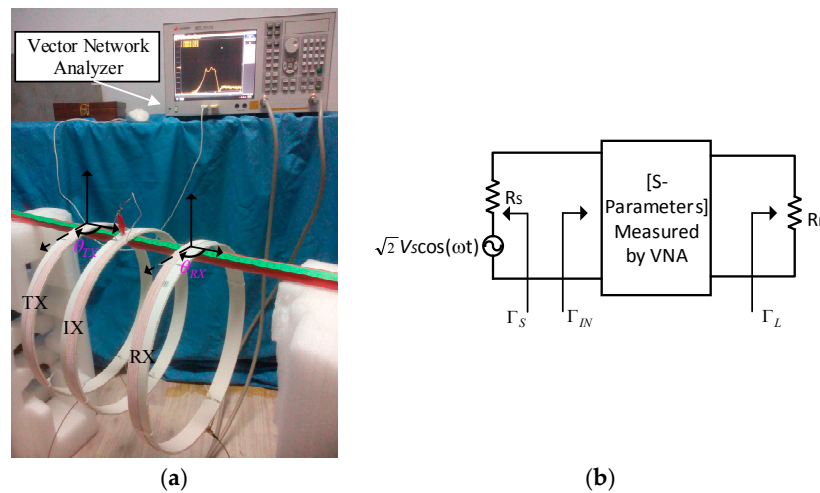


Figure 9. Experimental setup: (a) Measurement platform; and (b) Block diagram of a two-port network is terminated by arbitrary R_S and R_L for calculating the PTE and PDL of the measuring system.

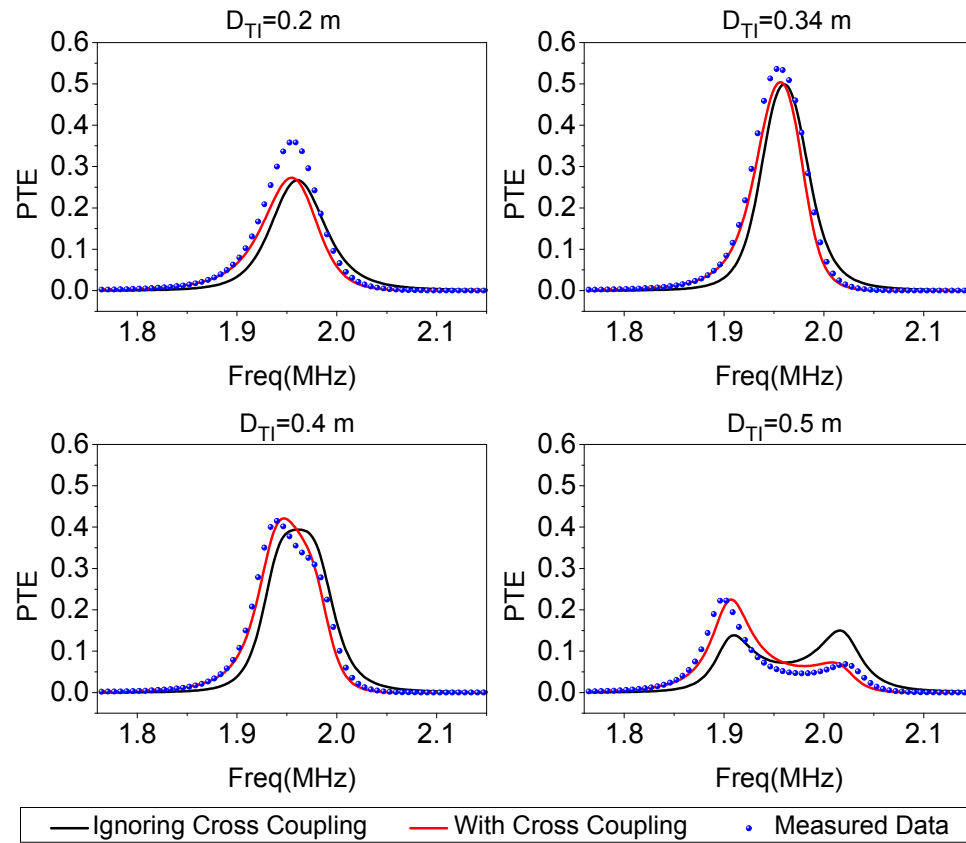
4.2. Measured Results Comparing with Theoretical Values

4.2.1. Verification of the Analysis of Three-Resonator Wireless Power Transfer System

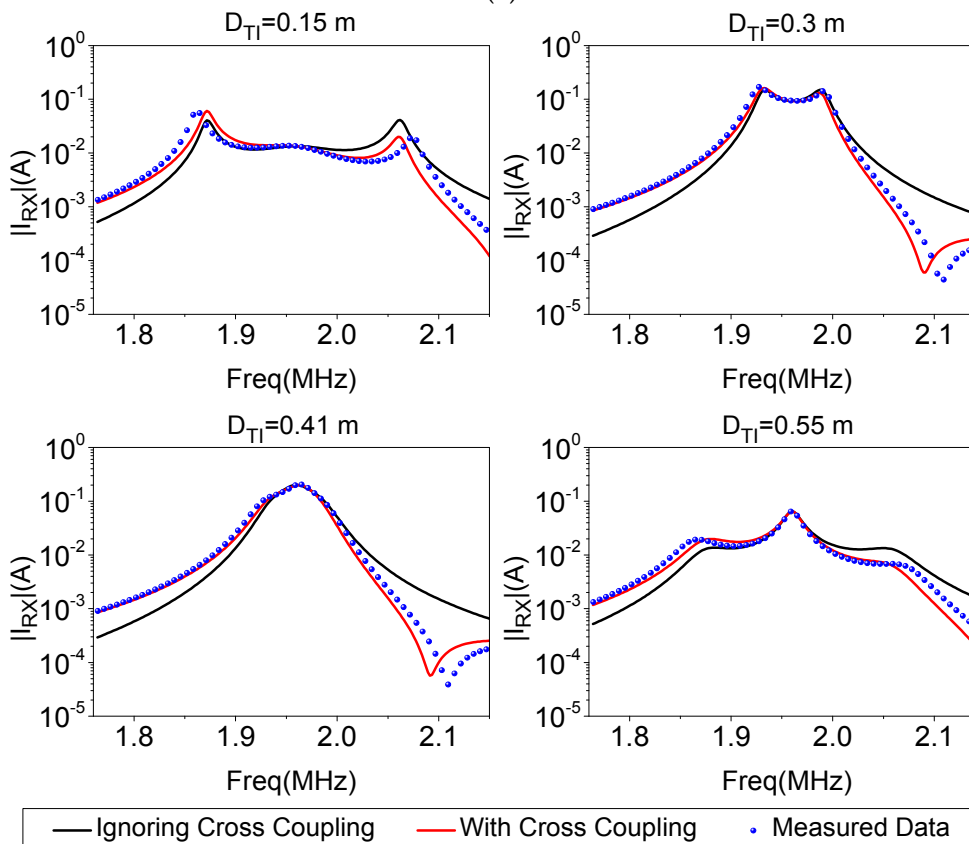
The case in Section 2.3 is measured to verify the analysis of the energy transfer characteristics in three-resonator WPT system. Theoretical results with and without considering the effects of the cross coupling, compared with measured counterparts at four representative inserted distances for PTE and PDL, are shown in Figure 10. From Figure 10a, the measured datum at $D_{TI} = 0.2, 0.34$ and 0.4 m, which are located in the theoretical non-frequency splitting region ($D_{TI} < 0.41$ m) of PTE, each of them has only one local maximum value of PTE; and at $D_{TI} = 0.5$ m located in the theoretical frequency splitting region ($D_{TI} > 0.41$ m), the measured curve has two local maximum values of PTE. Similarly in Figure 10b, the measured datum at $D_{TI} = 0.15$ and 0.55 m located in the theoretical frequency splitting region with three splitting frequencies of PDL ($D_{TI} < 0.212$ m and > 0.536 m) and at $D_{TI} = 0.3$ m located in the theoretical frequency splitting region with two splitting frequencies of PDL (0.212 m $< D_{TI} < 0.373785$ m) have three and two local maximum values of PDL, respectively. Transmission characteristic of PDL at $D_{TI} = 0.3$ m indicates that the verdict of achieving maximum power transmission always at original resonant frequency in three-resonant system presented in [8] is inaccurate. At the distance of $D_{TI} = 0.41$ m in non-frequency splitting region, only one maximal measured value of PDL appears. All of these demonstrate that two splitting frequencies arise at most for local maximum PTE in a three-resonator WPT system, and three or two splitting frequencies would appear for local maximum PDL when relative positions of TX, IX and RX are changed.

4.2.2. Verification of the Feasibility for Predetermined-Goals Wireless Power Transfer in Three-Resonator System

To realize the three kinds of predetermined-goal WPT in practical measurement, the optimal values of k for these goals achieved in the aforementioned procedure are transformed into tuning angle $\theta = [\theta_{TX}, \theta_{RX}]$. Setting $S = 0$ m in Figure 3, the coupling coefficient, k , between two coils versus rotation angle of Coil 2, θ , at different transfer distances, D , are calculated using Equations (10) and (11) and plotted in Figure 11.



(a)



(b)

Figure 10. Measured and theoretical results of three-resonator WPT system under collinear axes arrangement scenario at different inserted distance, D_{TI} , when transfer distance $D_{TR} = 0.7$ m: (a) PTE vs. frequency; and (b) $|I_{RX}|$ vs. frequency.

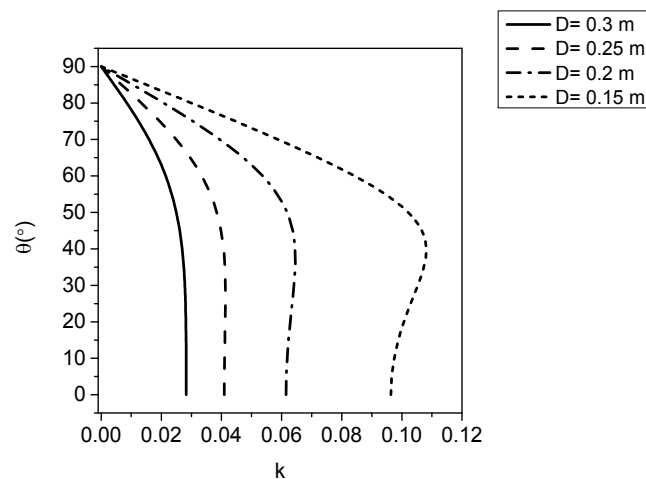


Figure 11. Angle, θ , vs. coupling coefficient, k , at different distances, D , without lateral misalignments of the two coils in Figure 3.

Using the case in Section 2.3, at $D_{TI} = 0.45$ m, The measured and calculated values of PTE of collinear axes arrangement scenario and maximizing PTE goal by tuning angle vector to $\theta = [\theta_{TX}, \theta_{RX}] = [0^\circ, 75.4^\circ]$, which is the optimal angle for maximum PTE according to Figures 6b and 11, are shown in Figure 12a. It can be seen that measured results agree with the calculated ones of system model with considering the cross coupling between TX and RX, and maximal PTE at original resonant frequency 1.96 MHz of maximizing PTE goal by tuning rotation angle of TX and RX is higher than the counterpart at low splitting frequency of collinear axes arrangement scenario using frequency tracking method. Using the same case, similar comparison for PDL of collinear axes arrangement scenario and maximizing PDL goal by tuning angle vector to $\theta = [\theta_{TX}, \theta_{RX}] = [79.7^\circ, 0^\circ]$ at $D_{TI} = 0.3$ m are included in Figure 12b. We can also find that maximal PDL of maximizing PDL goal is higher than that of collinear axes arrangement scenario.

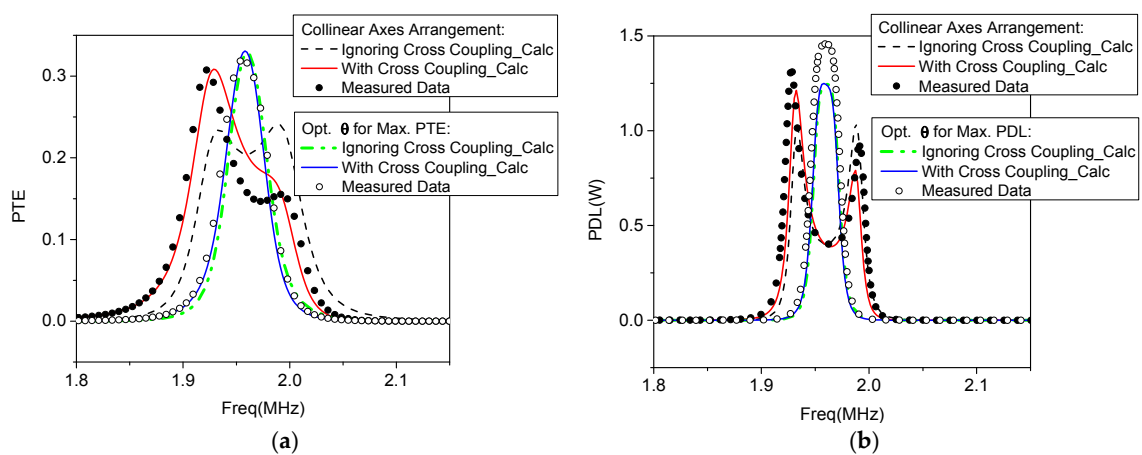


Figure 12. (a) Measured and theoretical PTE of collinear axes arrangement scenario and maximizing PTE by optimizing θ at $D_{TI} = 0.45$ m when transfer distance $D_{TR} = 0.7$ m; (b) Measured and theoretical PDL of collinear axes arrangement scenario and maximizing PDL by optimizing θ at $D_{TI} = 0.3$ m when transfer distance $D_{TR} = 0.7$ m.

Using the case in Section 2.3, at inserted distance $D_{TI} = 0.2, 0.31, 0.4$ and 0.55 m, the rotation angles of TX and RX are tuned to $[84.3^\circ, 0^\circ], [0^\circ, 0^\circ], [0^\circ, 78.5^\circ]$ and $[0^\circ, 87.7^\circ]$ for the predetermined-goal of achieving a constant PDL transfer of $PDL_C = 0.5$ W. The measured and theoretical values of PTE and PDL versus frequency for this predetermined-goal are shown in Figure 13. When IX moves close to TX

($D_{TI} = 0.2$ m) or close to RX ($D_{TI} = 0.55$ m), measured results of PDL at original resonant frequency (1.96 MHz) slightly deviate from preset power value 0.5 W. The reason is that the tuning angle θ for $D_{TI} = 0.2$ or 0.55 m is near 90° where the coupling coefficient k is sensitive to θ (see curves of $D = 0.2$ or 0.15 m in Figure 11), which results in inexact tuning angles and makes the measurement results inaccurate. The frequencies for the local maximum of model with cross coupling are consistent with the counterparts of model ignoring cross coupling at $D_{TI} = 0.2, 0.4$ and 0.55 m. The reason is because small cross coupling between TX and RX is achieved by tuning rotation angles of TX and RX. By combining the analysis results of the $D_{TR} = 0.7$ m case in Figure 8 with the measured results in Figure 13, it can be verified that PTE obtains its maximum value with preset PDL of 0.5 W at $D_{TI} = 0.31$ m, where optimal angle vector $\theta = [0^\circ, 0^\circ]$.

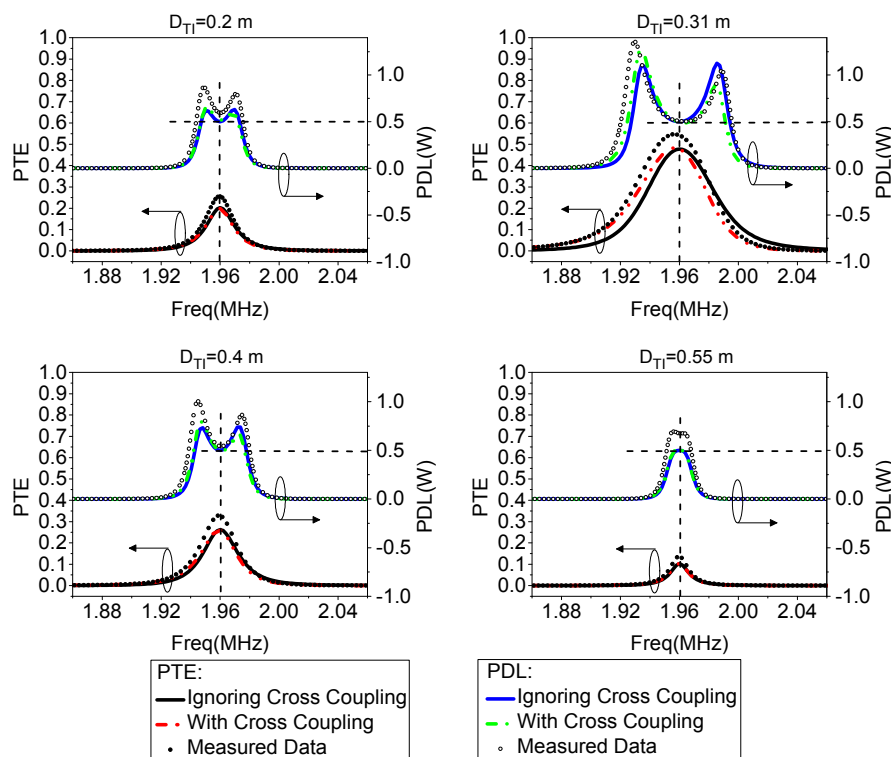


Figure 13. Measured and theoretical results of the predetermined-goal of obtaining a constant PDL at $f_0 = 1.96$ MHz when transfer distance $D_{TR} = 0.7$ m.

According to Figure 8 and the analysis for this figure and the verification result in Figure 13, the PTE maximizes at an optimal inserted distance D_{TI} when optimal angle vector $\theta = [0^\circ, 0^\circ]$ for a certain transfer distance D_{TR} . At original resonant frequency of 1.96 MHz, calculated and measured values of PTE and PDL of the third optimizing goal with two preset constant PDL_C of 0.5 W and 1 W, obtained with optimal D_{TI} and $\theta = [0^\circ, 0^\circ]$, are shown in Figure 14b,c. In the case of $PDL_C = 0.5$ W, the D_{TR} is effective to obtain this predetermined PDL for up to a distance of 1.16 m; however, when $PDL_C = 1$ W, the effective working distance is maximized at 0.99 m. This result indicates that the effective transmission distance D_{TR} decreases as PDL_C increases. The ratio of optimal D_{TI} to D_{TR} for the two constant PDL_C are plotted in Figure 14a. As can be seen from this figures, if transfer distances between TX and RX are at closer ranges, such as $D_{TR} < 0.76$ m and 1.07 m for $PDL_C = 0.5$ W and 1 W respectively, the optimal inserted positions of IX should be set close to TX, *i.e.*, $D_{TI}/D_{TR} < 0.5$; if not, the optimal inserted positions of IX are placed closed to RX. From Figure 14b,c, PTEs of model with cross coupling are nearly consistent with those of model ignoring cross coupling, and PDLs of the two models are increasingly differ with decreasing D_{TR} because of the increasing effects of cross coupling between TX and RX. However, it is effective using the proposed optimal method to achieve

the preset constant PDLs at maximum PTEs starting from $D_{TR} = 0.4$ m and 0.5 m for $PDL_C = 0.5$ W and 1 W respectively, for the maximum offsets below $PDL_C = 0.5$ W at $D_{TR} = 0.4$ m and $PDL_C = 1$ W at $D_{TR} = 0.5$ m are 12.9% and 9.21% respectively. The effects of cross coupling on energy transfer can be addressed through power flow analysis [22]. The power flow from TX and IX to Rx can be calculated by $P_{TR} = \text{Re}(-j\omega M_{TR} I_{TX} I_{RX}^*)$ and $P_{IR} = \text{Re}(-j\omega M_{IR} I_{IX} I_{RX}^*)$, respectively. Power loss in resonator of RX is $P_{Loss_RX} = -|I_{RX}|^2 R_3$. In Figure 15, the curves of P_{TR} , P_{IR} , P_{Loss_RX} and PDL ($PDL = P_{TR} + P_{IR} + P_{Loss_RX}$) are plotted versus D_{TR} when $PDL_C = 1$ W and 0.5 W, respectively. It can be observed that the power delivered from IX to RX (P_{IR}), which is affected gradually by cross coupling with decreasing D_{TR} , mainly determines the volume of PDL.

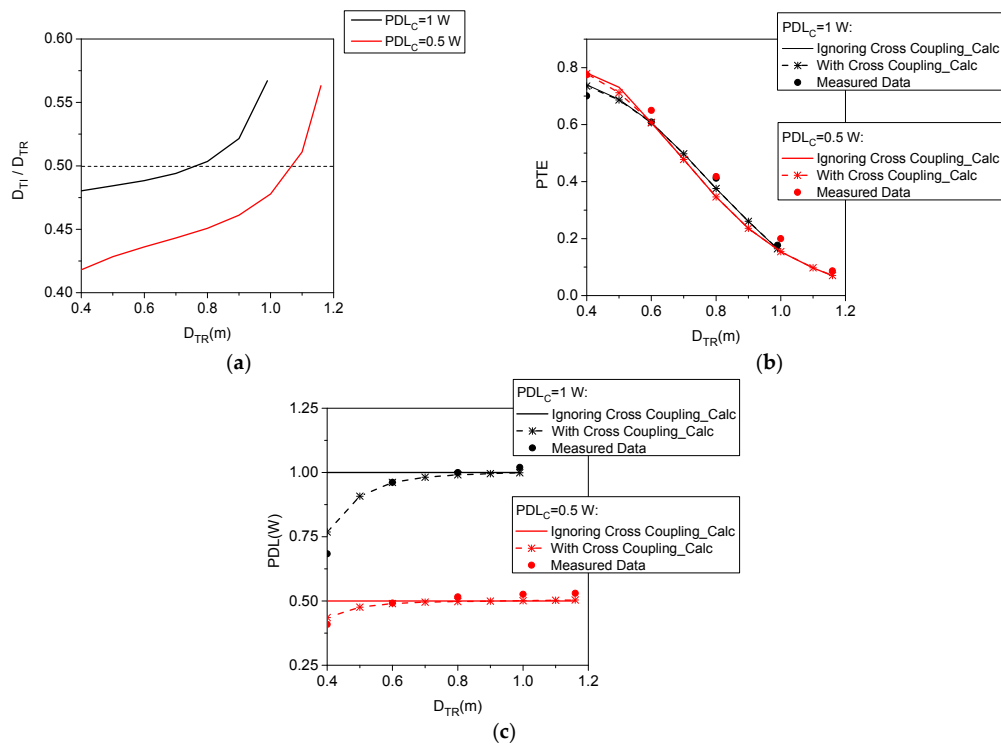


Figure 14. Energy transfer of obtaining predetermined constant PDL at maximum PTE at 1.96 MHz when $PDL_C = 1$ W and 0.5 W: (a) Ratio of optimal D_{TI} to D_{TR} vs. D_{TR} ; (b) Comparison between the calculated and measured values of PTE; and (c) Comparison between the calculated and measured values of PDL.

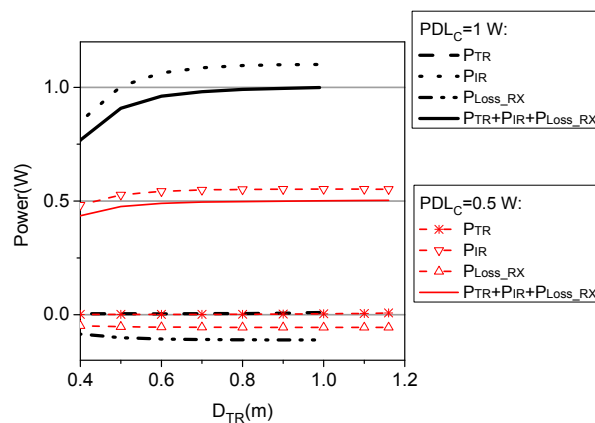


Figure 15. Power delivered to RX and power loss in it at 1.96 MHz under considering cross coupling model when $PDL_C = 1$ W and 0.5 W.

5. Conclusions

In this paper, we have introduced three parameters to derive concise formulations of the PTE and PDL based on coupled circuit model of three-resonator WPT system. Frequency splitting characteristics and calculating formulas for splitting frequencies of PTE and PDL are achieved by diagram discriminance. It has been proven via theoretical analysis and experimental measurement that there are non-frequency splitting region and frequency splitting region with two splitting frequencies for PTE, and non-frequency splitting region and frequency splitting region with two and three splitting frequencies for PDL. By transfer characteristic analysis of simplified circuit model and tuning rotation angles of TX and RX, an optimizing method using basic optimization algorithm is presented to achieve three predetermined-goals WPT of maximizing PTE transfer, maximizing PDL transfer and obtaining a constant amount of PDL transfer at maximum PTE at original resonant frequency. Comparing with frequency tracking method, the first two goals of maximizing PTE or PDL based on the proposed optimizing method can achieve higher PTE or PDL at different D_{TI} . Experimental results have demonstrated the effectiveness of the proposed method. For the third optimizing goal, theoretical analysis and experimental results show that the maximum PTE always appears at tuning angles of $\theta = [\theta_{TX}, \theta_{RX}] = [0^\circ, 0^\circ]$ and an optimal D_{TI} with a certain D_{TR} . The effect of cross coupling on power transfer is further analyzed based on power flow analysis.

For three-resonator WPT system, this investigation provides a deeper understanding of the WPT characteristics. The proposed optimizing method can effectively improve the PTE or PDL, especially for a fixed transmission distance case and can obtain a constant PDL transfer at maximum PTE for different transmission distance.

Acknowledgments: This research work was supported in part by the National Natural Science Foundation of China (61501257 and 61501258), Natural Science Foundation of Jiangsu Province of China (BK2012433 and BK20130872) and Nanjing University of Posts and Telecommunications Foundation of China (Grant No. NY 208037).

Author Contributions: Jin Zhang proposed the idea, performed the experiments, analyzed the data, and wrote the paper. Chonghu Cheng provided measuring tools and contributed to the discussion of this study.

Conflicts of Interest: The authors declare no conflict of interest.

References

1. Xia, M.; Sonia, A. On the efficiency of far-field wireless power transfer. *IEEE Trans. Signal Proc.* **2015**, *63*, 2835–2847. [[CrossRef](#)]
2. Zhang, J.; Cheng, C.H. Investigation of Near-Field Wireless Power Transfer between Two Efficient Electrically Small Planar Antennas. In Proceedings of the 2014 3rd Asia-Pacific Conference on Antennas and Propagation (APCAP), Harbin, China, 26–29 July 2014; pp. 720–723.
3. Liu, C.; Hu, A.P.; Nair, N.K.C. Modelling and analysis of a capacitively coupled contactless power transfer system. *IET Power Electron.* **2011**, *4*, 808–815. [[CrossRef](#)]
4. Zhen, Z.; Chau, K.T. Homogeneous wireless power transfer for move-and-charge. *IEEE Trans. Power Electron.* **2015**, *30*, 6213–6220.
5. Moorey, C.; Holderbaum, W.; Potter, B. Investigation of high-efficiency wireless power transfer criteria of resonantly-coupled loops and dipoles through analysis of the figure of merit. *Energies* **2015**, *8*, 11342–11362. [[CrossRef](#)]
6. Gao, Y.; Farley, K.B.; Tse, Z.T.H. A uniform voltage gain control for alignment robustness in wireless ev charging. *Energies* **2015**, *8*, 8355–8370. [[CrossRef](#)]
7. RamRakhyani, A.K.; Lazzi, G. On the design of efficient multi-coil telemetry system for biomedical implants. *IEEE Trans. Biomed. Circuits Syst.* **2013**, *7*, 11–23. [[CrossRef](#)] [[PubMed](#)]
8. Ahn, D.; Hong, S. A study on magnetic field repeater in wireless power transfer. *IEEE Trans. Ind. Electron.* **2013**, *60*, 360–371. [[CrossRef](#)]
9. Zhang, F.; Hackworth, S.A.; Fu, W.; Li, C.; Mao, Z.; Sun, M. Relay effect of wireless power transfer using strongly coupled magnetic resonances. *IEEE Trans. Magn.* **2011**, *47*, 1478–1481. [[CrossRef](#)]

10. Zhang, X.; Ho, S.; Fu, W. Quantitative design and analysis of relay resonators in wireless power transfer system. *IEEE Trans. Magn.* **2012**, *48*, 4026–4029. [[CrossRef](#)]
11. Kim, J.; Son, H.-C.; Kim, K.-H.; Park, Y.-J. Efficiency analysis of magnetic resonance wireless power transfer with intermediate resonant coil. *IEEE Antennas Wirel. Propag. Lett.* **2011**, *10*, 389–392. [[CrossRef](#)]
12. Zhong, W.X.; Zhang, C.; Xun, L.; Hui, S.Y.R. A methodology for making a three-coil wireless power transfer system more energy efficient than a two-coil counterpart for extended transfer distance. *IEEE Trans. Power Electron.* **2015**, *30*, 933–942. [[CrossRef](#)]
13. Sun, L.; Tang, H.; Zhang, Y. Determining the frequency for load-independent output current in three-coil wireless power transfer system. *Energies* **2015**, *8*, 9719–9730. [[CrossRef](#)]
14. Miyamoto, T.; Komiyama, S.; Mita, H.; Fujimaki, K. Wireless Power Transfer System with a Simple Receiver Coil. In Proceedings of the 2011 IEEE MTT-S International Microwave Workshop Series on Innovative Wireless Power Transmission: Technologies, Systems, and Applications (IMWS), Kyoto, Japan, 12–13 May 2011; pp. 131–134.
15. Awai, I.; Ikuta, Y.; Sawahara, Y.; Yangjun, T.; Ishizaki, T. Applications of a Novel Disk Repeater. In Proceedings of the 2014 IEEE Wireless Power Transfer Conference (WPTC), Jeju, Korea, 8–9 May 2014; pp. 114–117.
16. Kiani, M.; Jow, U.-M.; Ghovanloo, M. Design and optimization of a 3-coil inductive link for efficient wireless power transmission. *IEEE Trans. Biomed. Circuits Syst.* **2011**, *5*, 579–591. [[CrossRef](#)] [[PubMed](#)]
17. Uei-Ming, J.; Ghovanloo, M. Design and optimization of printed spiral coils for efficient transcutaneous inductive power transmission. *IEEE Trans. Biomed. Circuits Syst.* **2007**, *1*, 193–202.
18. Islam, A.B.; Islam, S.K.; Tulip, F.S. Design and optimization of printed circuit board inductors for wireless power transfer system. *Circuits Syst.* **2013**, *4*, 237–244. [[CrossRef](#)]
19. RamRakhyani, A.K.; Mirabbasi, S.; Chiao, M. Design and optimization of resonance-based efficient wireless power delivery systems for biomedical implants. *IEEE Trans. Biomed. Circuits Syst.* **2011**, *5*, 48–63. [[CrossRef](#)] [[PubMed](#)]
20. Ahn, D.; Hong, S. Wireless power transmission with self-regulated output voltage for biomedical implant. *IEEE Trans. Ind. Electron.* **2014**, *61*, 2225–2235. [[CrossRef](#)]
21. Villa, J.L.; Sallan, J.; Sanz Osorio, J.F.; Llombart, A. High-misalignment tolerant compensation topology for ICPT systems. *Ind. Electron.* **2012**, *59*, 945–951. [[CrossRef](#)]
22. Zhang, J.; Cheng, C.H. Quantitative investigation into the use of resonant magneto-inductive links for efficient wireless power transfer. *IET Microw. Antennas Propag.* **2016**, *10*, 38–44. [[CrossRef](#)]
23. Babic, S.I.; Akyel, C. Calculating mutual inductance between circular coils with inclined axes in air. *IEEE Trans. Magn.* **2008**, *44*, 1743–1750. [[CrossRef](#)]
24. Sample, A.P.; Meyer, D.A.; Smith, J.R. Analysis, experimental results, and range adaptation of magnetically coupled resonators for wireless power transfer. *IEEE Trans. Ind. Electron.* **2011**, *58*, 544–554. [[CrossRef](#)]
25. Park, J.; Tak, Y.; Kim, Y.; Kim, Y.; Nam, S. Investigation of adaptive matching methods for near-field wireless power transfer. *IEEE Trans. Antennas Propag.* **2011**, *59*, 1769–1773. [[CrossRef](#)]
26. Pozar, D.M. *Microwave Engineering*, 3rd ed.; Wiley & Sons, Inc.: New, York, NY, USA, 2005.

